Experimental and numerical study of the size effect on compound Meso/Microforming behaviors and performances for making bulk parts by directly using sheet metals

Jun-Yuan Zheng[1], M.W. Fu[1, *], Jilai Wang[2]

[1] Department of Mechanical Engineering, The Hong Kong Polytechnic University, Hung Hom, Kowloon, Hong Kong SAR of China

[2]

* mmmwfu@polyu.edu.hk

Graphical abstract
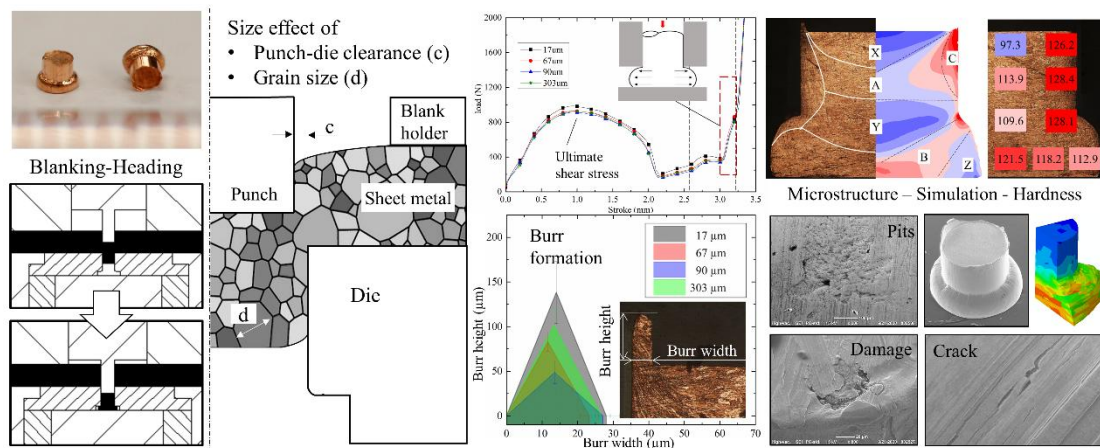
Highlights

1) A compound blanking-heading microforming system produces plug-shaped parts using sheet metals.

2) When punch-die clearance equals grain size, maximum ultimate shear stress and highest burr height are obtained.

3) More material shortage and smaller bulge diameter are got with larger grain size and clearance.

4) Hardness and microstructure of final parts differ with grain size and punch-die clearance.

5) Sunken area, pits, crack and surface damage on the bottom surface and crack on the bulge surface are observed.

Abstract

Sheet-based bulk microforming with compound tooling is an efficient approach to accomplish mass production of plug-shaped parts with high quality and productivity. However, size effect induces irregular mechanical responses and deformation behaviors in micro-scale. In this work, a compound microforming system for blanking-heading process was developed to produce micro-plug parts by directly using copper sheets. Different punch-die clearances and grain sizes of specimen were employed to study the interactive effects of geometrical and grain size on the microforming process and the final part. Through the experimental and numerical results and measurements of final parts, the influences of size effect on the microstructural evolution, geometrical precision and surface defects of final parts and the load-stroke relationship during forming process were symmetrically investigated. The results reveal that when punch-die clearance equals grain size, the maximum ultimate shear stress of blanking and the highest burr are obtained. The larger grain size and punch-die clearance increase the material shortage and reduce the bulge diameter of final parts. Three shear bands and three dead metal zones are recognized on the cross-section of parts, and various defects including sunken area, pits, crack and damage are observed on the surface of parts. These findings facilitate the production of plug-shaped microparts in the aspects of process monitoring and product qualities control and enrich the understanding of sheet-based bulk compound microforming.

Keywords: Progressive and compound microforming, micro bulk forming of sheet-metals, size effect, microstructural evolution, forming defects.

1. Introduction

Micro-manufacturing technologies and metallic micro-parts have developed and matured in the last decade to meet the increasing demands of product miniaturization in industrial fields [1]. The traditional micro-manufacturing technologies including micro-machining [2, 3], micro-EDM [4], photolithography [5] and laser machining have capabilities to fabricate micro-parts with high precision and desirable qualities, but they are not suitable for mass production because of their cost and the material limits. Microforming has become the spotlight for mass production among all micro-manufacturing technologies because of its high productivity and efficiency, less material waste, good net-shape or near-net-shape characteristic of final parts and economic and environmental-friendly production [6-8]. To solve the troubles in handling, transporting and ejection among different forming processes, the concept of progressive and compound forming is proposed. This unique process aims on the complex-structure or multi-feature parts formed using sheet metal. The term "progressive" means that a particular processing chain with two or more single forming steps and progressive dies are employed, and each step has its designed stroke and predefined task, so that several forming steps can be conducted together with multiple efficiency [9]. The term "compound" is to combine several types of material deformation into one single stroke rather than one in a regular forming step. Many prior researches related to progressive and compound forming were conducted. Fu and Chan [10] developed a two-scaled progressive micro/meso-forming system to examine the grain and geometrical size effect on the micro/meso-flanged parts. Meng et al. [11] studied the grain size effect and fracture criteria in progressive double-flanging microforming process. Meng et al. [12] extensively investigated the micro-ironing progressive microforming process and the related characteristic of microparts and deformation behaviors. Zheng et al. [9] further developed a four-step progressive microforming system to fabricate conical-flanged parts, and studied the geometrical and grain size effect in the forming process and the part quality. Tang et al. [13] investigated the multi-stage deformation in progressive microforming and the

properties of final parts considering material crystal structures and grain sizes. Zheng et al. [14, 15] explored the potential of progressive microforming in industrial production, and studied its fabrication of micro pin-shaped parts instead of conventional micro-machining process through the aspects of required tolerance, surface roughness and material-flow-affected strength considering grain size effect and structure design. Ran et al. [16] studied the dead metal zone inducing dislocation strengthening effect and ductile fracture in progressive microforming through producing an extrusion-punching formed cylindrical parts. Fu et al. [17] developed a blanking-drawing compound microforming process to form micro-cups and investigate the size effect on forming load and thickness distribution. Chan et al. [18] conducted a compound double-extrusion microforming test and investigated the relationship between material flow, friction and deformation load of the forming process.

However, the knowledge and experience in macro-forming cannot be applied in the downscaled microforming process directly, since "size effect" changes the material deformation behaviors and mechanical properties from macro-scale to micro-scale [19]. Prior investigations of size effect were conducted mainly from the aspects of geometrical, microstructural and tribological size effects in different types of microforming process. Chan et al. [20] conducted micro-heading considering grain and feature size effect to investigate the microstructural revolution and material flow behaviors. Chen et al. [21] conducted a precision micro-forging process to fabricate micro-gears using wire-EDM cutting micro-gear mold, and focused on the surface quality and dimensional deviation of mold and the forming accuracy and productivity of micro-gears. Su et al. [22] studied the interactive effects of grain size and temperature on the formability and part quality of micro-embossing process, and clarified the plastic deformation mechanisms and intragranular dislocation movement based on misorientation angle distribution. Sato et al. [23] developed a hydromechanical based deep-drawing microforming process to study the accuracy and drawability of drawn cups, where the applying appropriate counterpressure can

eliminate the generation of wrinkles and reduce the friction. Wang et al. [24] conducted a micro-deep drawing process using conical die with multi-layered film coating, and studied the tribological size effect on the surface quality and the uniform distribution of micro-conical parts. Guo et al. [25] analyzed the earing evolution in micro deep drawing considering the interactive effect of crystal plasticity and surface layer model, and they revealed the earing profile of formed cup differed with grain size, orientation and specimen thickness. Kardan et al. [25] conducted a micro-upsetting process using crystal plasticity theory and investigated the grain orientation affected geometrical shapes. Lou et al. [26] attempted to explore the formability and product properties using ultrasonic-assisted micro-extrusion to fabricate micro-pins.

Many prior researches on size effect have been extensively conducted based on numerical methods, and among them, crystal plasticity finite elements method (CPFEM) is one of the popular methods, whose feasibility and precision has been verified. CPFEM considers the texture and grains distribution to study the deformation behaviors of crystal, which can present the heterogeneity for coarse-grained materials [27]. Many researchers conducted numerical and experimental works using CPFEM. Yalcinkaya et al. [28] proposed a model to address statistical size effect due to random grain orientation and the effect of grain boundary conditions. Zhang et al. [29] used high-resolution crystal plasticity simulation to investigate the anisotropic yield behavior with four yield functions of polycrystalline aluminum alloy. Ghosh and Cheng [30] developed a micro-twin nucleation-propagation model to study HCP material based on CP simulation with a novel subcycling algorithm. Cai et al. [31] investigated the yielding behavior in biaxial tensile tests considering size effect and hard phase effect. Wang et al. [32] studied anisotropic deformation in ultra-precision diamond cutting of polycrystalline copper combing Johnson-Cook damage model for material removal. Fischer et al. [33] studied the thermo-mechanical properties of the honeycomb structure during rubbing.

Although numerous studies about microforming and size effect were conducted,

it still lacks an in-depth investigation on size effects in the compound microforming and the sheet-based bulk microforming. Plug-shaped parts are also common and popular in micro-products, so how to efficiently produce plug-shaped parts is deserved to research. In this study, a compound microforming system including micro-blanking and micro-heading operations was developed to fabricate micro-plug parts using sheet metals, and the influence of grain size and blanking clearance on the micro blanking-heading process and the forming quality of final parts are comprehensively studied from the aspects of forming load, burr formation, dimensional precision, material flow behavior, hardness distribution, surface defects formation and geometrical profile variation. The crystal plasticity based simulation was conducted to compare with the homogeneous properties based simulation to evaluate the surface curve variation. The results show that higher grain size and thicker punch-die clearance reduce the forming load, worsen the material shortage, and decrease the bulge diameter. The material flow behavior is discussed based on the hardness test and the microstructural evolution with numerical results. The radius variation of heading feature is predicted well by crystal plasticity model. Surface defects including sunken area, crack, damage and pits are observed and their formation and elimination are discussed. All these findings in this study thus enrich the knowledge and understanding of blanking-heading compound microforming and sheet-based bulk microforming to support the design and fabrication of plug-shaped or other bulk-formed microparts and compound tooling design and facilitate the wide application of the compound microforming process as an efficient way compared to conventional micro-manufacturing technologies.

2. Experimental details and simulation setup

2.1 Testing material and mechanical properties

T1 pure copper (Cu $\geqslant$ 99.95%) is selected in this study due to its excellent formability and other good mechanical properties. Pure copper sheets (20×90 mm)

with thickness of 2 millimeters are annealed under different heat treatment conditions, and then cooled down to room temperature by air in the argon-filled furnace to obtain diverse grain sizes. The microstructures of pure copper along the thickness direction after annealing are illustrated in **Fig. 1**, and their annealing conditions and corresponding grain sizes are shown in **Table 1**. The cross-section of specimen is cut, grinded, polished, and then etched by solution of 5 g $FeCl_3$, 85 ml H_2O and 15 ml HCl. The grain sizes are measured according to the linear intercept method of ASTM E112 standard.

To quantitatively analyse the mechanical response of the testing materials, micro-cylindrical specimens are cut from the pure copper sheets by EDM to conduct uniaxial compression tests. The specimens are 1.2 mm in diameter and 2 mm in height. Lubricant grease is used to reduce friction. Strain rate of 0.002 s^{-1} is employed for quasi-static deformation. Each group contains four repeated tests. The true stress versus true strain curves are illustrated in **Fig. 2**(a). It is revealed that the flow stress reduces with the increase of grain size. As shown in **Fig. 2** (b), the flow stress of tested materials meets the Hall-Petch mechanism well below strain of 0.4, which indicates the linear relation between the stress and the inverse square root of grain sizes. For polycrystal model, the extending Hall-Petch relationship [34] is widely applied to describe the flow stress in the following:

$$\overline{\sigma}(\overline{\varepsilon}) = \sigma_0(\overline{\varepsilon}) + k(\overline{\varepsilon}) \cdot d^{-1/2} \tag{1}$$

where $\overline{\sigma}$ is flow stress, $\overline{\varepsilon}$ is effective strain, σ_0 and k are constant for a given $\overline{\varepsilon}$, and d is grain size.

| 500°C-2h | 750°C-2h | 800°C-3h | 950°C-3h |

——————— 100 μm
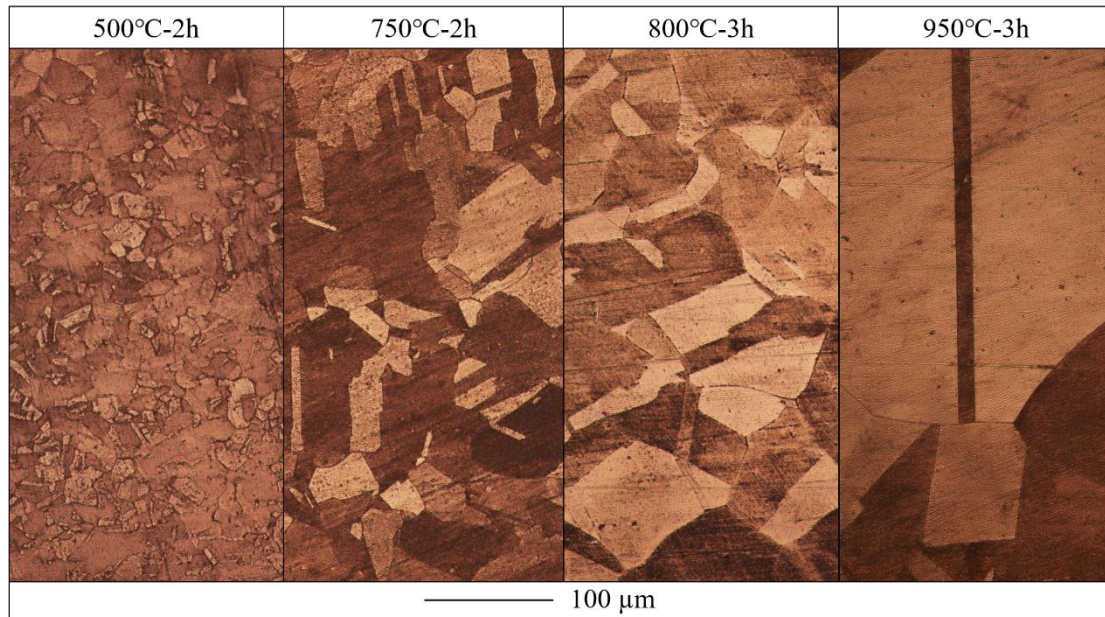
Fig. 1 Microstructures of pure copper along thickness direction under different annealing conditions.

Table 1 Annealing conditions and the related grain sizes of pure copper.

Temperature (℃)	500	750	800	950
Holding time (hrs)	2	2	3	3
Grain size (μm)	17 ± 2	67 ± 3	90 ± 8	303 ± 7
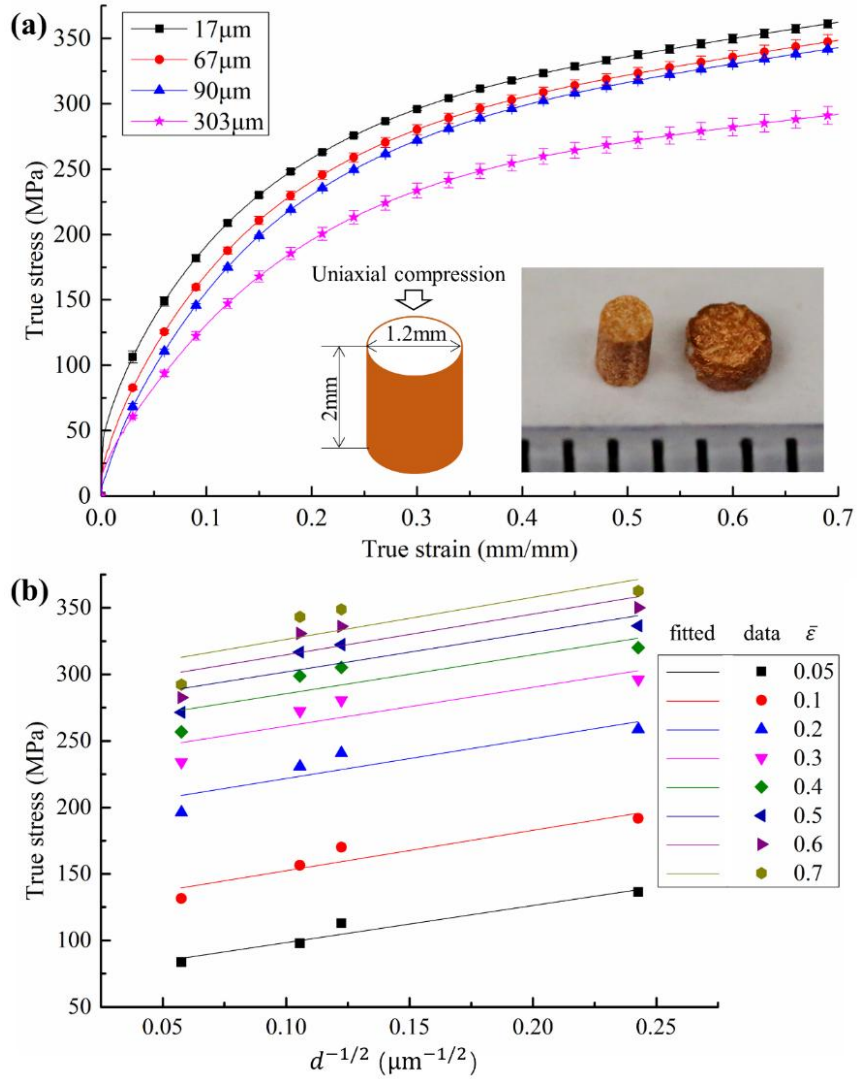
Fig. 2 (a) Stress-strain curves of pure copper with different grain sizes; (b) Hall-Petch relationship.

2.2   Material properties in CPFEM

To numerically study the inhomogeneous deformation during the compound microforming process, CPFEM considering the material texture is employed in simulation. Crystal plasticity is a physically based plasticity theory that presents the plastic deformation of metal in micro-scale. The dislocation in a metallic crystal along slip systems is represented in a continuum framework [27]. Plastic strain is assumed to be solely due to crystallographic dislocation slips. The lattice of a crystalline material undergoes elastic deformation and rotation. Its plastic deformation is assumed to be induced by crystalline slip. The material flows through the crystal

lattice by dislocation motion. The total deformation gradient $\boldsymbol{F}$ is as follows:

$$\boldsymbol{F} = \boldsymbol{F}^e \boldsymbol{F}^p \tag{2}$$

where $\boldsymbol{F}^p$ is plastic shear deformation to an intermediate reference configuration whose lattice orientation and spacing are the same as in the original reference configuration, and $\boldsymbol{F}^e$ denotes the stretching and rotation of the lattice. The decomposition of Eq.(2) along with the velocity gradient $\boldsymbol{L}$ is shown as follows:

$$\begin{cases} \boldsymbol{L} = \dot{\boldsymbol{F}}\boldsymbol{F}^{-1} = \boldsymbol{L}^e + \boldsymbol{F}^e \boldsymbol{L}^p \boldsymbol{F}^{e-1} \\ \qquad \boldsymbol{L}^e = \dot{\boldsymbol{F}}^e \boldsymbol{F}^{e-1} \\ \qquad \boldsymbol{L}^p = \dot{\boldsymbol{F}}^p \boldsymbol{F}^{p-1} \end{cases} \tag{3}$$

where $\boldsymbol{L}^e$ and $\boldsymbol{L}^p$ are the elastic and plastic distortion rates, respectively.

Introducing the Schmid law, the plastic distortion rate is summed up by the shearing rates on each active slip system as follows:

$$\boldsymbol{L}^p = \sum_{\alpha} \dot{\gamma}^{\alpha}(\boldsymbol{s}^{\alpha} \otimes \boldsymbol{m}^{\alpha}) \tag{5}$$

where $\boldsymbol{s}^{\alpha}$ and $\boldsymbol{m}^{\alpha}$ are the unit vector along slip direction and the normal to the slip plane of the αth slip system in the intermediate reference configuration. $\boldsymbol{s}^{\alpha} \otimes \boldsymbol{m}^{\alpha}$ is the Schmid factor of the active slip system. $\dot{\gamma}^{\alpha}$ is the plastic shear strain rate in the αth slip system. The resolved shear stress τ^{α} on the αth slip system can be expressed as [35]:

$$\tau^{\alpha} = \boldsymbol{F}^e \cdot \boldsymbol{F}^{eT} \cdot \boldsymbol{S} : (\boldsymbol{s}^{\alpha} \otimes \boldsymbol{m}^{\alpha}) \tag{6}$$

where $\boldsymbol{S}$ is the second Piola-Kirchhoff (PK2) stress tensor. In addition, the rate-dependent kinetic law for face-centered cubic (fcc) metallic crystals is used in this research, where the shearing rate $\dot{\gamma}^{\alpha}$ of the αth slip system is shown as follows [36]:

$$\dot{\gamma}^{\alpha} = \dot{\gamma}_0 \left| \frac{\tau^{\alpha}}{g^{\alpha}} \right|^{1/m} sgn(\tau^{\alpha}) \tag{7}$$

where $\dot{\gamma}_0$ is the reference strain rate, g^{α} is the current strength of the αth slip system, and m is the rate sensitivity parameter, respectively. g^{α} develops with the

accumulation of dislocation in a crystal with work-hardening. Its rate $\dot{g}^\alpha$ can be calculated by:

$$\dot{g}^\alpha = \sum_\beta h_{\alpha\beta} |\dot{\gamma}^\beta| \tag{8}$$

where $h_{\alpha\alpha}$ $(\alpha = \beta)$ and $h_{\alpha\beta}$ $(\alpha \neq \beta)$ are the self and latent slip hardening moduli, respectively. The latent hardening modulus is obtained by:

$$h_{\alpha\beta} = q h_{\alpha\alpha} \tag{9}$$

where q is a factor representing the relationship between slip systems.

The Kalidindi's hardening formulation [37] for self-hardening module is selected in this work, which is expressed as:

$$h_{\alpha\alpha} = h_0 (1 - \frac{g^\alpha}{\tau_s})^a \tag{10}$$

where h_0 is the initial hardening modulus, τ_s is the shear stress where large plastic flow initiates, and a is the rate sensitivity of the rate of strain hardening.

In addition, the elastic tensor constants for pure copper are that C_{11} = 168.4 GPa, C_{12} = 121.4 GPa, and C_{44} = 75.4 GPa, respectively [38].

The other parameters of the pure copper in this study are presented in **Table 2**

Table 2 Parameters for pure copper [37] in this study.

τ_0(MPa)	τ_s(MPa)	h_0(MPa)	$\dot{\gamma}_0(s^{-1})$	m	a	q
16	148	180	0.001	0.012	2.25	1.4

In the CPFEM simulation, the quarter-cylindrical parts with height of 2 mm and radius of 0.6 mm are symmetrically fixed on X and Y direction and then compressed by 60% in height-direction. The polycrystal model is generated through software Neper with grain size of 303 μm. Three repeated simulations are conducted. The

stress-strain curve for grain size of 303 µm obtained from simulation compared with the relative experimental data is illustrated in **Fig. 3**. The true stress is measured from the applied force divided by the immediate area, and the true strain is calculated from the total accumulative shear strain. It can be seen the mechanical response in the simulation using Kaladinli et al.'s parameters [37] is fitted well with the experimental data obtained from uniaxial compression tests when the strain is below 0.4, so the simulation results in this research are reliable.
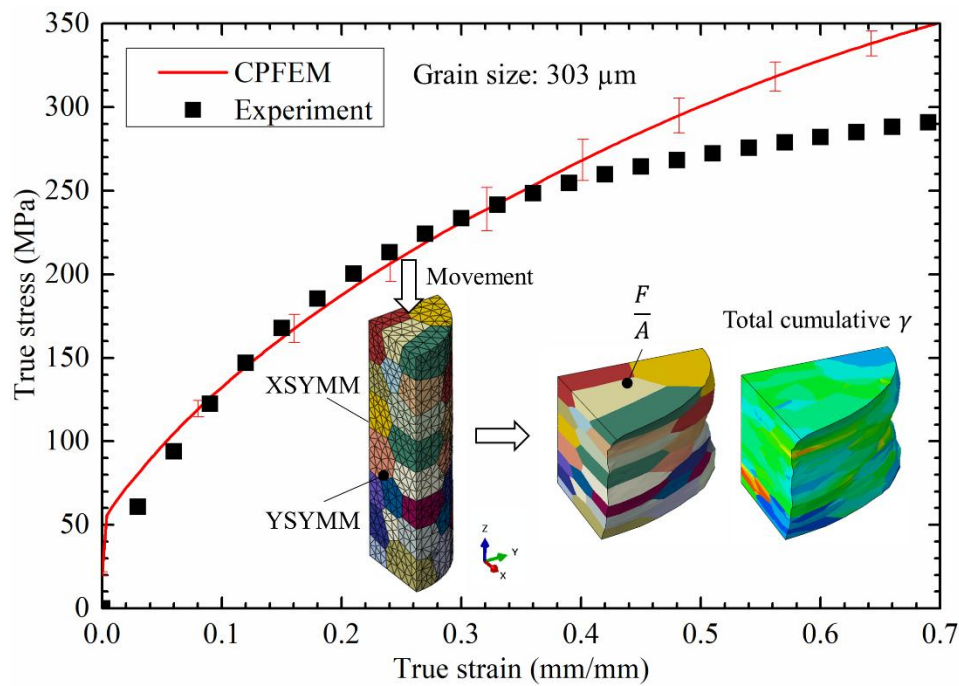
Fig. 3 Stress-strain curve of CPFEM and experimental data for grain size of 303 µm and its simulation method.

2.3   *Micro plug part and realization of compound microforming*

The design and dimensions of the micro plug part with the compound microforming system are illustrated in **Fig. 4**. The compound microforming system is installed between the upper and lower platform equipped on an MTS testing machine with 50kN maximum capacity load cell. Punches with different diameters are employed in the compound forming process to study the geometrical size effect of punch-die clearance. The punch-die clearances in each case are presented in **Table 3**. Pure copper sheets with different initial grain sizes are used as specimen to study the

grain size effect in the compound forming process. The compound microforming process and the relative dimensions of mold are shown in **Fig. 5**. At the beginning of process, the specimen is insert in the slot between blank holder and die holder, and the blank holder is screw up to avoid shaking during the forming process. Then the compound forming process starts. The material undergoes shearing deformation during the blanking stage, and a micro-cylindrical part is cut from the specimen at the finish of this stage. With the punch continuous moving, the heading stage begins. The trimmed cylindrical part is compressed to fill the die cavity, where extrusion deformation happens. The desirable geometry is formed at the end of this stage. Then the insert die releases, and the formed part is ejected. The specimen moves forward, and a new forming process starts. Machine oil is used as lubrication on each interface to minimum friction. The punching speed is 0.01 mm/s, so the effect of strain rate can be neglected.
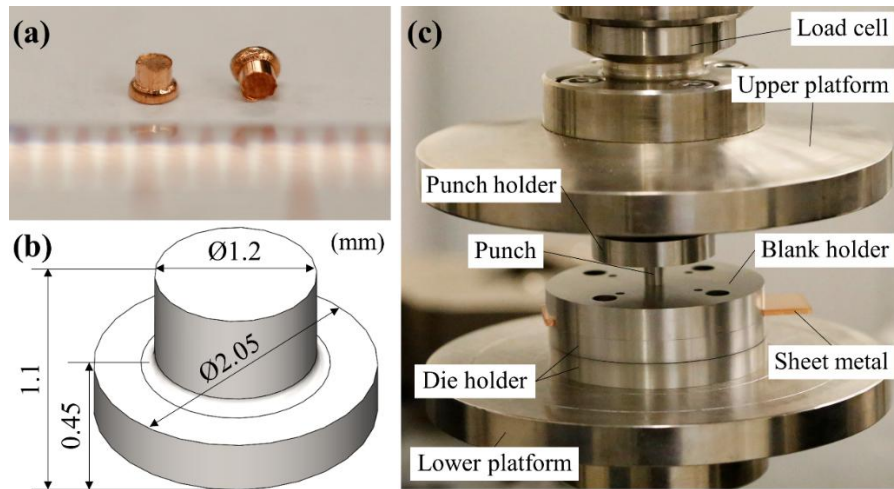
Fig. 4 (a) Photo of final parts; (b) design of the micro plug parts; and (c) photo of the compound microforming system.

Table 3 Punch-die clearances of different punches.

	Case 1	Case 2	Case 3
Punch diameter (mm)	1.192	1.140	1.090
Die diameter (mm)		1.230	

Clearance on each side (µm)	19	45	70
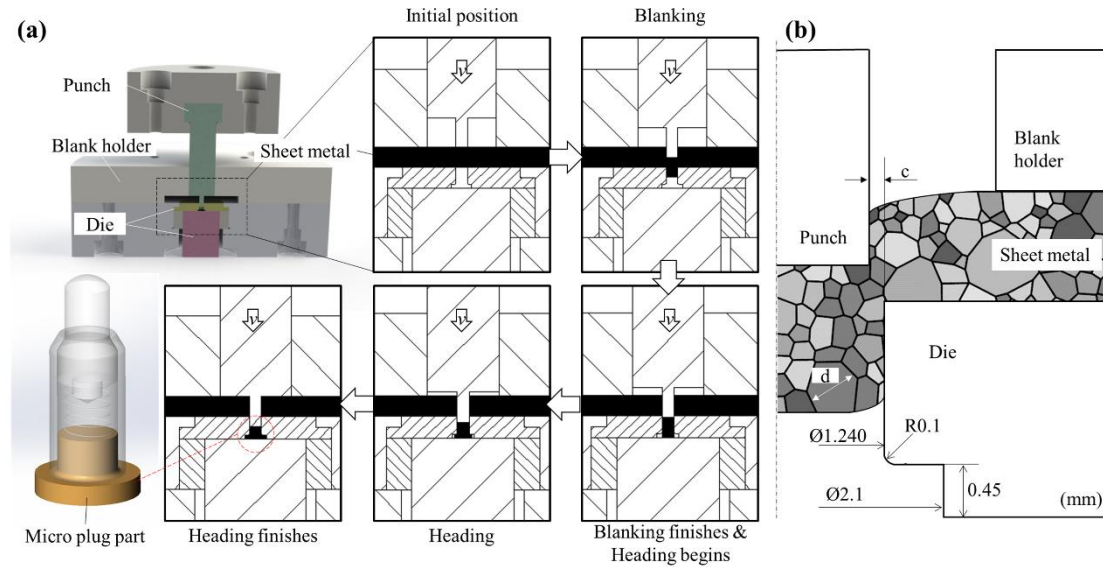
Fig. 5 (a) The compound microforming system and the forming steps; (b) The dimensions of dies.

3.   Result and discussion

3.1   *Load-stroke relationship during the compound microforming*

Micro-punching and micro-blanking are both shearing operation, which differs in producing micro-cylinders or micro-holes [39]. The shearing operation is divided into three stages, which are the rising elastic-plastic stage, the static shearing deformation stage, and the dropping fracture stage [10]. The results in **Fig. 6** (a-c) meet the prior studies about grain size effect in micro-punching/blanking process [9, 10, 14, 40], in which the punching load/pressure decreases with the increase of grain size, since the barrier-like characteristic of grain boundaries during shearing deformation decrease with the increase of grain size. **Fig. 6** (d) shows the effect of punch-die clearance (c) on the forming load in micro-punching/blanking process. The forming load increases with the decrease of clearance, which correlates with the prior studies [41, 42]. Ultimate shear stress (σ_s) is introduced as $\sigma_s = F_{max}/\pi dl$, where F_{max}, d, l are the maximum blanking load, punch diameter and the length of blanked surface. Xu et al.

[8] indicated the clearance / grain size ratio (c/d) and clearance / thickness ratio (c/t) are both main factors influencing the deformation behaviors of micro-punching/blanking. When c/d = 1, the ultimate sharing strength reaches a maximum value. In this study, as shown in **Fig. 7**, the main impact to ultimate shear stress is still punch-die clearance, where the ultimate shear stress increase with the increase of punch-die clearance, It is because the involved material volume of shearing deformation occupies the major effect on shearing stress. On the other hand, when the punch-die clearance is 19 μm, the ultimate shear stress reaches the maximum value with c/d ≈ 1, and for the other two clearances, the increasing slope obviously gets steady when c/d > 1, it is speculate a maximum value at c/d = 1 but influenced by the complicated force and friction condition. When c/d > 1, grains are evenly distributed in lateral and thickness direction, the main mechanism in the shearing deformation is grains coordinating deformation. With the increase of grain size, the grains coordinating deformation become difficult, and grain boundary sliding and grain rotation show their obviousness, which makes the ultimate shear stress increases. Conversely, when c/d < 1, the deformation mechanism is related to the grain lattice and slip. Thus, the number of grains on the thickness direction is important. The more grains involved in deformation, which means the increasing c/d ratio, the harder to make the deformation along the critical resolved shear stress (CRSS) direction of single crystal, which enhances the ultimate shear stress. Therefore, when c/d = 1, the ultimate shear stress should reach the maximum value according to the two deformation mechanisms.
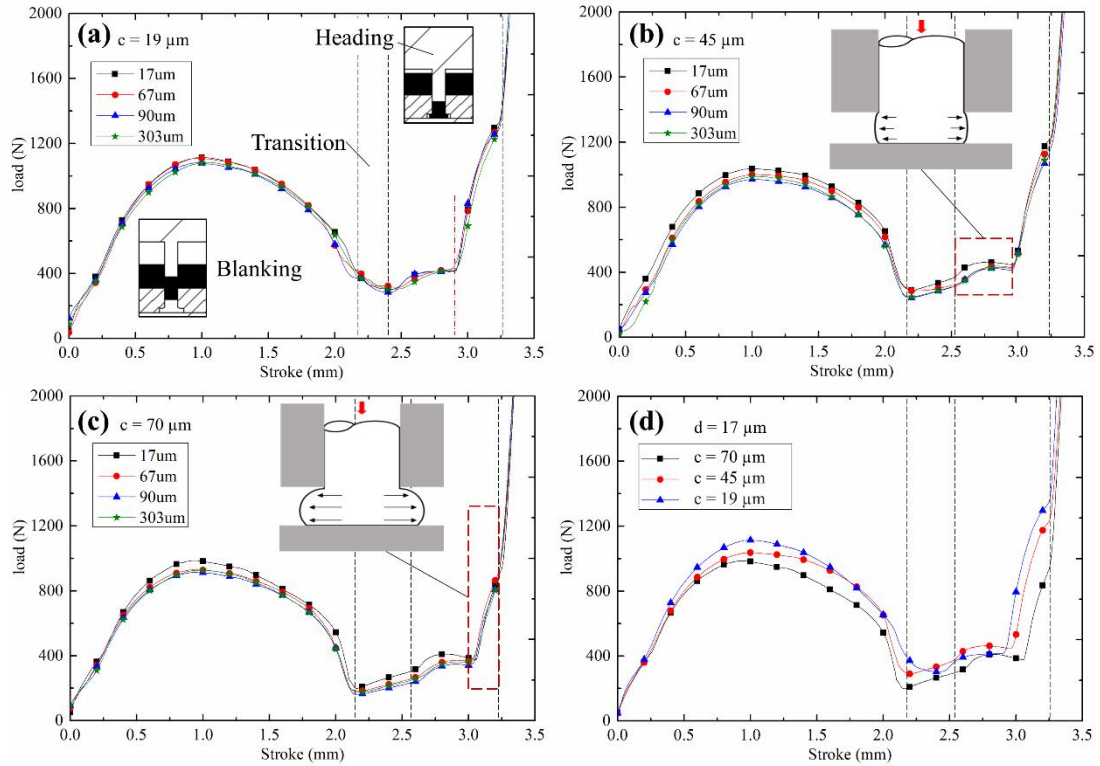
Fig. 6 Load-stroke curves with different punch-die clearances of (a) 19 µm, (b) 45 µm and (c) 70 µm, and (d) load-stroke curves with specific grain size of 17 µm.
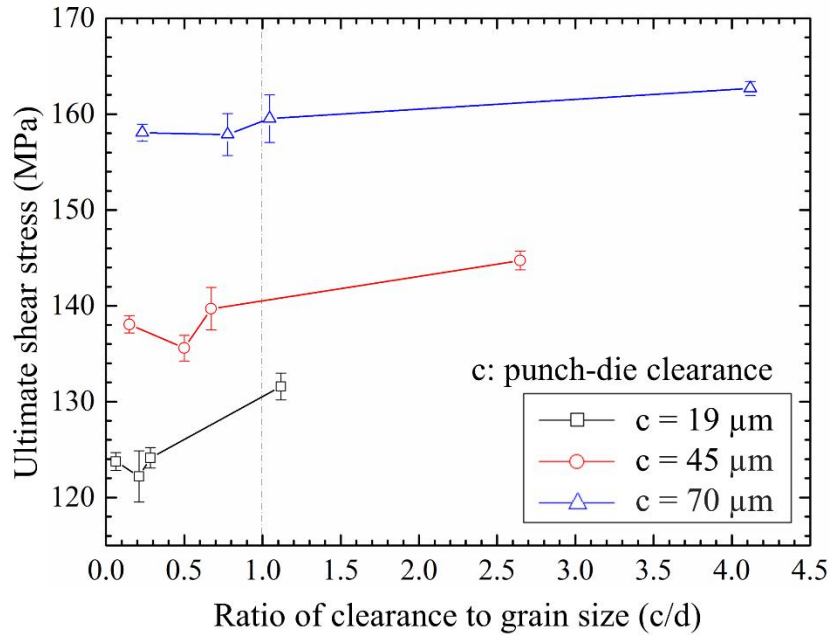
Fig. 7 Ultimate shear stress during blanking stage with different c/d ratio.

Besides the shearing stage, transition and heading stages are recognized from the load-stroke curves in **Fig. 6**. The transition stage starts after the blanking operation finishes and ends of the heading operation begins. The load in this stage is mainly

caused by the friction of micro-cylindrical part sliding in the die central hole. Moreover, the curves in heading stage start with a short peak, which is the first heading stage, then rise quickly in a parabolic shape, which is the second one, and they roar rapidly when the punch reaches the designed stroke limitation. In the first heading stage, the material is subjected to elastic-plastic deformation and slightly bulged. With the punch movement, the plastic deformation is promoted severely, and the interfacial friction between material and die increase until the extrusion finishes. Grain size effect is not significant in this stage. However, as shown in **Fig. 6** (d), punch-die clearance (c) can greatly affect the load and stroke in this stage, where the forming load in second heading stage increases with a smaller punch-die clearance. The geometrical size effect is the result of the different volume of cylindrical parts after blanking, where the larger punch-die clearance induces shorter and thinner blanked cylinder, thus its deformation in heading stage is decreased relatively, and lower forming load is generated.

3.2   Microstructural evolution

The microstructural evolution of microparts includes the formation of shear band and the remained dead metal zone (DMZ). Dead metal zone is defined as no or almost no material flow zone, which is related to the geometry of die, interfacial property and loading rate [14, 43-45]. Understanding microstructural evolution is important to predict the mechanical properties of final parts and the material flow behaviors during forming process. The recognition of dead metal zones is generally dependent on hardness measurement and flow lines distribution on the cross-section of the etched micrographs. In this work, the study of microstructural evolution is conducted detailly from experimental hardness test and numerical simulation of strain distribution. The results from two aspects are discussed to reveal material flow behaviors in this compound microforming.

3.2.1   Hardness distribution

The test of hardness distribution reveals the work hardening in the compound

microforming process. This material strengthening phenomenon is the result of generation and movement of dislocation within crystal structure and grain boundary sliding of material. Vickers hardness test on the cross-section of formed parts was conducted to evaluate the work hardening accumulation during compound microforming process. The test results are illustrated in **Fig. 8**. As shown in **Fig. 8** (a), the original hardness of fine-grained material (17 μm) is slightly higher than it of other grain sizes. From the variation of hardness on cross-section, as shown in **Fig. 8** (b-e), it can be seen that the higher hardness appears near the lateral profile of the cylindrical feature, which is induced by the shearing deformation in the blanking operation. The hardness near the corner of heading-formed feature slightly drops, and obviously reduces at the widest tip. Conversely, the central area at the top of part has the lowest hardness, and this value drops with the increase of grain size. Along the symmetrical line downward, there are two peaks of hardness, which indicates two separated shear bands. The first one is on the mid-upper area, from the center elongating to the lateral profile, and the other one locates on the center of bottom surface extending to the corner on profile. However, in the very-coarse-grained material (303 μm), the mid-upper shear band disappear., which is caused by less strain accumulation on large grains. By the comparison among different grain sizes, it is revealed that the hardness on undeformed area drops significantly and the hardness on shear band slightly decreases with coarser grains, since the increasing number of grain boundaries enhances the work hardening effect. However, the hardness on cylindrical profile does not change a lot.
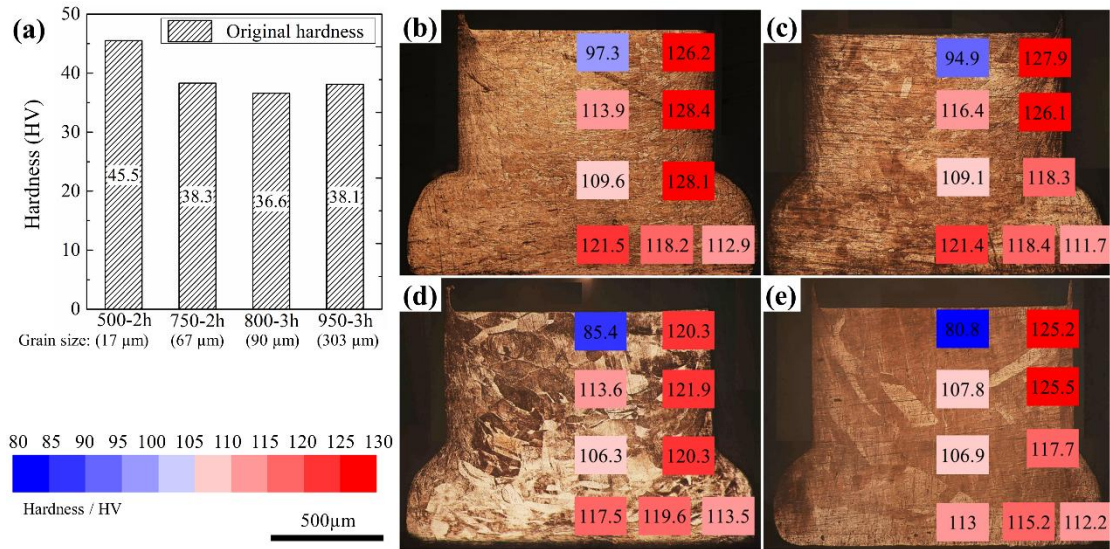
Fig. 8 (a) Initial hardness of specimen; hardness on different area of the cross-section of the formed parts with different grain size of (b) 17 μm, (c) 67 μm, (d) 90 μm and (e) 303 μm (HV).

3.2.2   Strain distribution

Numerical simulation was conducted through commercial software DEFORM based on uniaxial tensile test data to study the formation of shear bands and dead metal zones, and the results are compared with the flow line on the cross-section of final parts to study the influence of punch-die clearance, as illustrated in **Fig. 9**. As shown in **Fig. 9** (a-c), three shear bands, A,B,C, and three dead metal zones, X, Y, Z are recognized from the microstructures and numerical simulation of final parts with grain size of 17 μm. When the punch-die clearance is the smallest (19 μm), as shown in **Fig. 9** (a), it is clearly to configure the boundary between inherit zones. The grains in X and Y are nearly undeformed. Dead metal zone X is formed just below the flat punch because the material flow underneath flat punch in blanking is little. Grains in Zone Y are barely deformed during the micro-blanking process, and the horizonal elongating in heading does not affect them, thus Zone Y is kept after micro-heading. The arched shear band A is formed during micro-blanking operation between Zone X and Zone Y and extend to the shearing area. The material in A is subjected to tensile stress in horizonal direction, which transmits the punching load to the punch-die edge to make the shearing deformation happen. The findings are similar to the micro-blanked cylindrical part in Meng et al.'s study [46]. The shape and height of

Zone Y are mainly dependent on the shear band A and B.

In addition, shear band B is formed during the heading operation, where the bottom material is compressed and bulged in horizonal direction, but hindered by the punching hole, thus deformation is concentrated on the bottom edge of central hole, and extended to the central bottom surface with a compressive force. The grains in A and B are severely elongated along horizon direction and extend to shear band C, which is formed induced by severe shearing deformation during micro-blanking operation.

Moreover, the simulation results indicate a small dead metal zone Z on the bottom edge of the final parts, attributed to the gradually decreasing horizontal strain along horizontal direction from the central bottom surface to the edge during micro-heading. But this zone is not obvious on the microstructure figure.

With the different punch-die clearances, the microstructural evolution and strain distribution are different. In **Fig. 9** (b), where the punch-die clearance is 45 μm, the area of Zone X increase slightly, and the grains in Zone A and C rotate and extend more severely, as shown in the partial diagram **Fig. 9** (i). In addition, the boundary on microstructure between dead metal Zone Y and shear band B is fuzzy. It can be seen that the horizonal elongation of grains gradually increases in downward direction. The partial diagrams to present the grains in this area are **Fig. 9** (ii) and (iii).
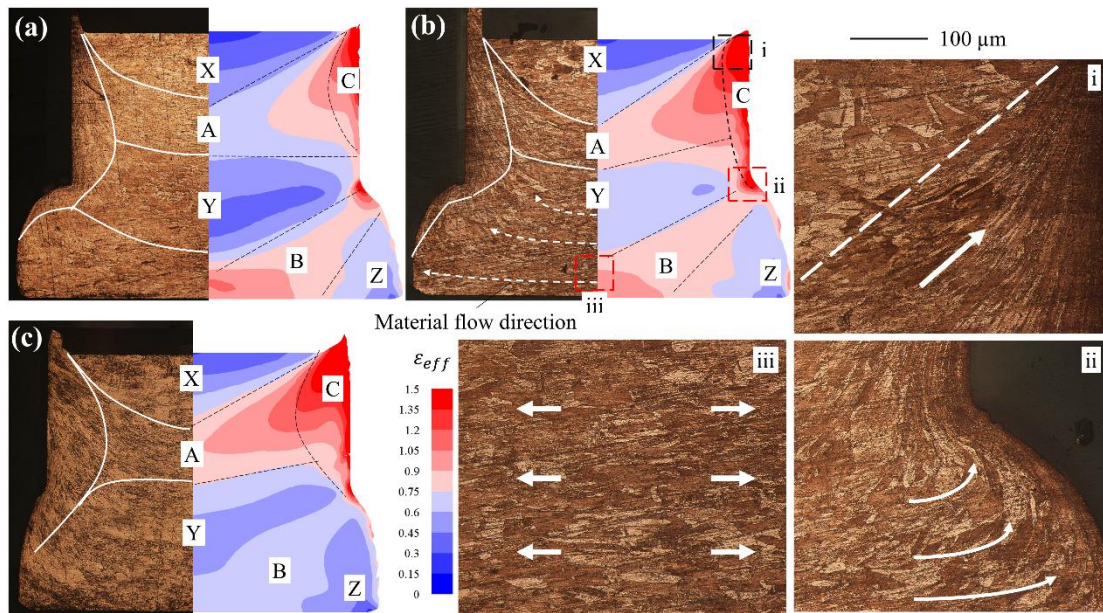
Fig. 9 Microstructures and effective strain on cross-section with grain size of 17 μm and punch-die clearance of (a) 19 μm, (b) 45 μm and (c) 70 μm; partial view on (i) top edge, (ii) corner and (iii) central bottom.

3.3   Geometrical precision

Geometrical precision of final parts is important for evaluating the characteristic of novel microforming process. In this work, the burr formation and dimensional accuracy of final parts are studied. Moreover, the material shortage during compound microforming process and radius variation in micro-heading are investigated.

3.3.1   Burr formation

Burr formation is generally induced by the clearance between punch and die during punching/blanking process. To quantitatively study the variation of burr in different grain sizes and punch-die clearances, the comparison of burr height and burr width is shown in **Fig. 10**. As shown in **Fig. 10** (b-d), where the punch-die clearance is fixed, the width of burr approximately equals the punch-die clearance, and the grain size has no obvious influence on the width of burr. In the diagrams **Fig. 10** (e-h), the effect of punch-die clearance on burr formation with a given grain size are presented. The triangular areas in the diagram can mediately indicate the volume of burr. It can be seen that the volume of burr is promoted significantly with higher punch-die

clearance.

In addition, to directly investigate the regularity of height of burr, the relationship between the clearance to grain size ratio (c/d) and the height of burr is illustrated in **Fig. 11**. It is revealed that, with a given punch-die clearance, when c/d ratio is around one, the longest burr is obtained. On the other hand, the lower punch-die clearance can slightly decrease the height of burr. With the smallest punch-die clearance (19 µm), the heights of burr are greatly decreased. The burr formation mechanism is related to the happening of material ductile fracture, which are influenced by c/d ratio. In macro-scale, the ductile fracture mechanism is based on that the microvoids initiate, microvoids growth perpendicular to stress direction, microvoids coalescence, and fracture. Since the microvoids are more possible to appear at the grain boundaries, the number of grains on deformation area is important to the fracture behaviors. When c/d > 1, grains have homogeneous distribution on thickness and clearance directions, and the fracture mechanism is related to the number of grain boundaries and microvoids. Thus, the larger c/d ratio, the more grains are involved in deformation, and the more microvoids initiate and growth, so the ductile fracture happens earlier, which results in a shorter burr. Conversely, when c/d < 1, individual grain dominates on clearance direction, and the fracture mechanism changes to the slip and dislocation within grain lattice. Thus, with the growth of grain size, the number of grains on the thickness direction is less, and the dislocation is easier to extend since grain boundary acts as barrier to obstruct dislocation, which results in earlier happening of ductile fracture. Therefore, when c/d = 1, the two ductile fracture mechanisms lead to the longest height of burr. However, due to the complicated interfacial conditions for burr formation including friction, surface roughness, and so on, the regularity is not generally applicable among different sets of punch and die, and there is a deviation for the clearance of 45 µm.
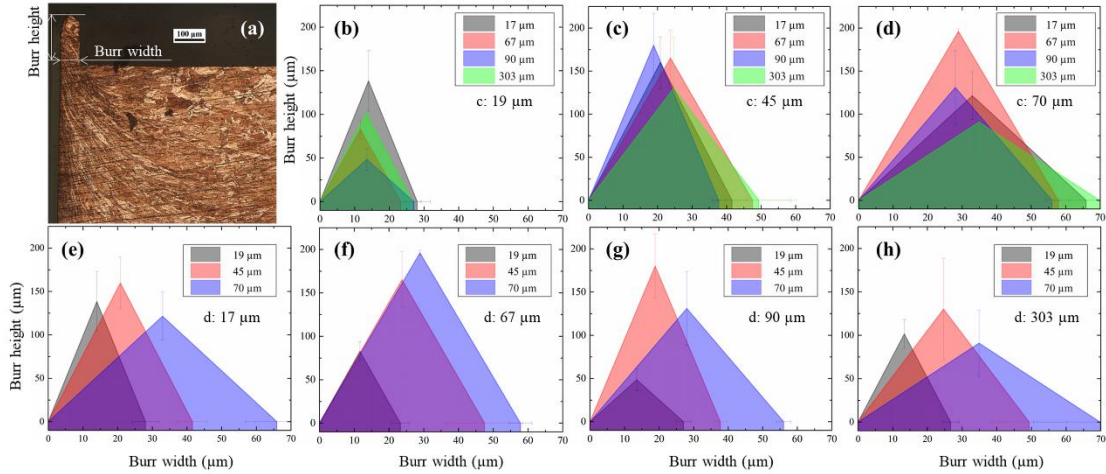
Fig. 10 (a) Burr illustration; height and width of burr at specific (b) – (d) punch-die clearance or (e) – (h) grain size.
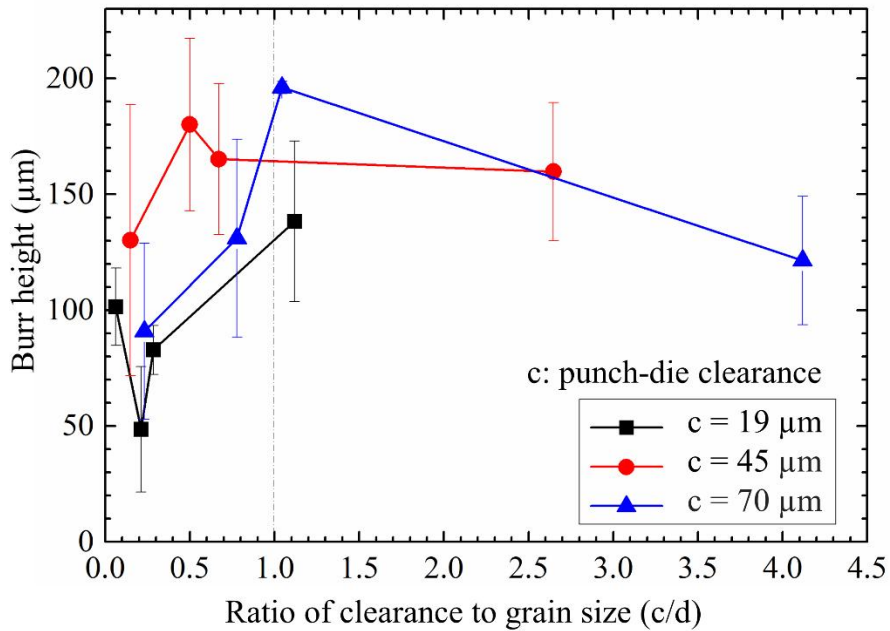
Fig. 11 Burr height of the final part with different c/d ratio.

3.3.1 Undesirable material shortage

In micro-punching/blanking process, the material cannot always flow along the desirable direction to form the designed geometries. Material lateral flow is a general phenomenon and gets worse with the coarser grains due to the inhomogeneous distribution. In this study, material shortage happening at the micro-blanking operation facilitate the undesirable geometry of the blanked cylinder including burr, rollover and height shortage. To quantitively study the material shortage during the

compound microforming, shortage fraction is introduced, which is:

$$Shortage\ fraction = \frac{1 - Effective\ volume}{Design\ volume}$$

where "effective volume" is the volume of the effective shape, and design volume is the volume of the designed part in **Fig. 4**. The variation of shortage fraction with different grain sizes and punch-die clearances is shown in **Fig. 12**. Due to the unavoidable height shortage and burr formation after micro-blanking, the minimum value of shortage fraction is still 33 percent. It shows an increase trend with larger grain size, since the lateral deformation increases with coarse-grained material. There is an obvious rising of shortage fraction with a larger punch-die clearance, since a larger punch-die clearance enhances the volume of burr, which further reduces the volume of effective shape.
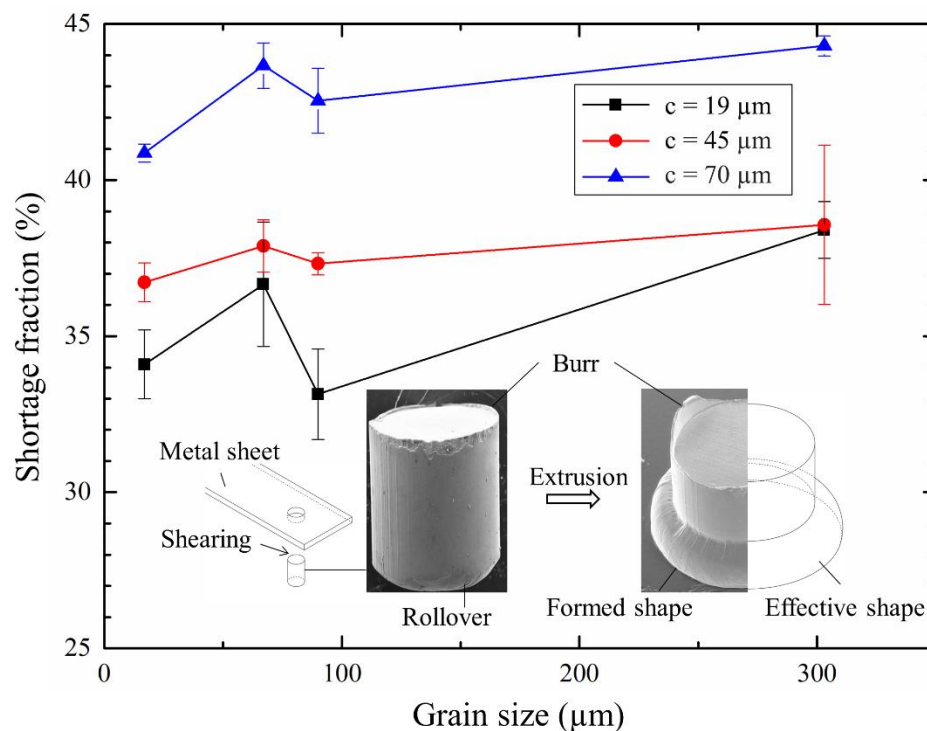
Fig. 12 Volume shortage fraction during the compound forming process.

3.3.2　Dimensional accuracy

Investigating the dimensional accuracy of final parts facilitate the improvement of tooling development, part and process design and process factor variation. Dimensional accuracy in microforming is more serious than it in macroforming, since

severe undesirable geometries and phenomena appear in small scale. To quantitively determine the grain and geometrical size effect, three critical dimensions of the micro plug parts are selected to present their variation with grain size and punch-die clearance, which are the height of parts (H), the average diameter of the cylindrical feature (D1), and the largest diameter of the bulge feature (D2), as shown in **Fig. 13** (a). The measured results are illustrated in **Fig. 13** (c-e) and grouped by different punch-die clearances. From these figures, it can be seen that the punch-die clearance and grain size show little influence on H and D1 (vary less than 50 um), but D2 shows a decreasing tendency with the increase of both grain size and punch-die clearance. **Fig. 13** (b) focuses on the variation of D2 with different grain size and punch-die clearance. It can be seen D2 shows linear decreasing trend with the increased grain size, and the interception decrease with the increase of punch-die clearance. Since the orientation of individual grain dominates the material properties with large grain size, the material is hard to flow along desirable direction during, which results in the height shortage of the blanked cylinder [9] and asymmetrical extrusion in micro-heading process. In addition, the decrease of the effective volume of blanked cylinder due to large punch-die clearance is another reason for D2 reduction.
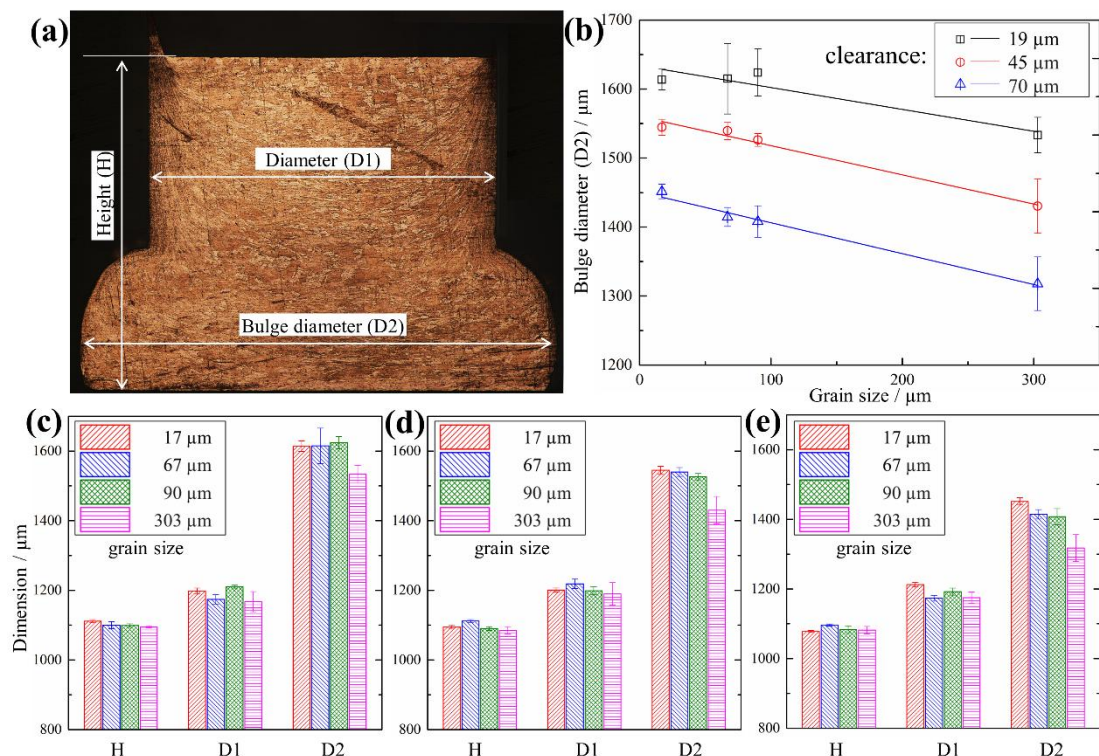
Fig. 13 (a) Dimensions of formed part; (b) variation of bulge diameter; dimension of each feature under different grain size and punch-die clearance of (c) 19 µm, (d) 45 µm and (e) 70 µm.

3.3.3　Radius variation during heading operation

CPFEM simulation was conducted based on the constitutive model in Section 2.2 and implemented through script and subroutine in software Abaqus. A finite element simulation based on homogeneous theory was conducted for comparison. The radius change in micro-heading operation is focused in this research, and the results of experiment, CPFEM simulation and FEM simulation are illustrated in **Fig. 14**. **Fig. 14** (a) and (b) shows the deviation of radius of the bottom surface of heading feature around perimeter and their relative standard deviation. It is revealed the FEM results are homogeneous, and CPFEM predicts properly the unevenness of experimental results, where their changing tendency are similar and their relative standard deviations are close. In addition, **Fig. 14** (c) and (d) present X and Y position of the measurement nodes in **Fig. 14** (e) with different punch strokes to show the roundness change. It can be seen that at about the half of total stroke, the roundness is apparently reduced for CPFEM model. The roundness for FEM model is always good.
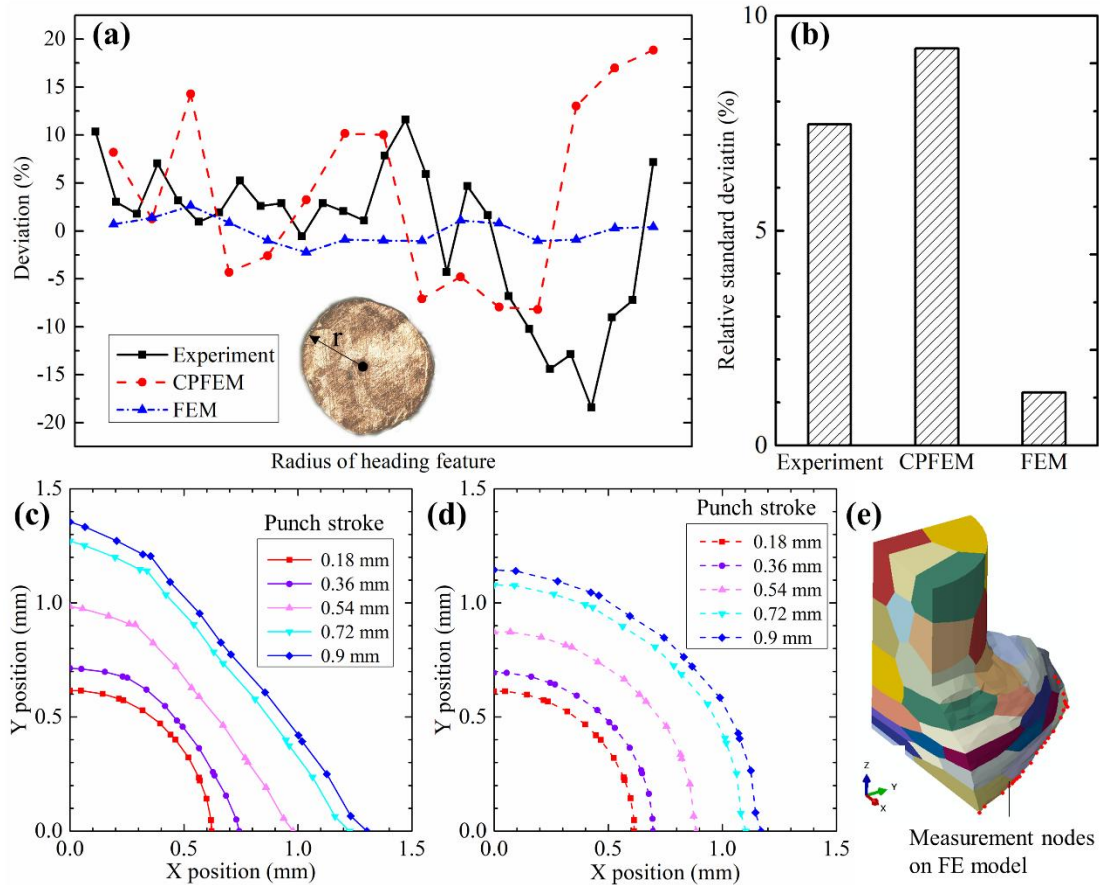
Fig. 14 (a) Radius change of the heading feature and (b) its relative standard deviation. The variation with punch stroke of X and Y position on (c) CPFEM model and (d) FEM model. (e) The illustration of measurement nodes.

Moreover, the distribution of effective stress and effective plastic strain of FEM and CPFEM simulation are shown in **Fig. 15**. As seen in **Fig. 15** (a), the stress and strain distributions of CPFEM are based on grain orientation, which are nonuniformly distributed. Conversely, FEM do not consider grain orientation. As a result, the CPFEM result, which respects to the microstructure of the material considering grain orientations, gets a more accurate results than it in FE. In addition, because of the assumption that material in the CPFE is inhomogeneous, the maximum values of stress and strain at certain area are recognized.
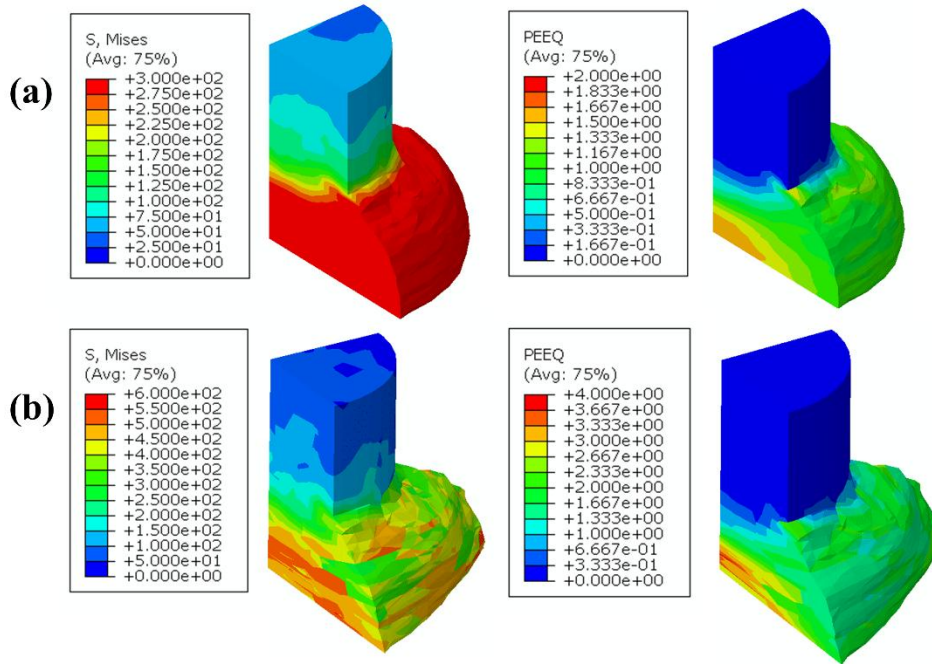
Fig. 15 Effective stress and effective plastic strain distribution for (a) FEM and (b) CPFEM.

3.4 *Surface defects*

The morphologies of final parts were observed by scanning electron microscope (SEM). **Fig. 16** shows the fine-grained parts with different punch-die clearance. The decrease of the diameter of heading feature and the increase of burr volume are apparent with larger punch-die clearance.
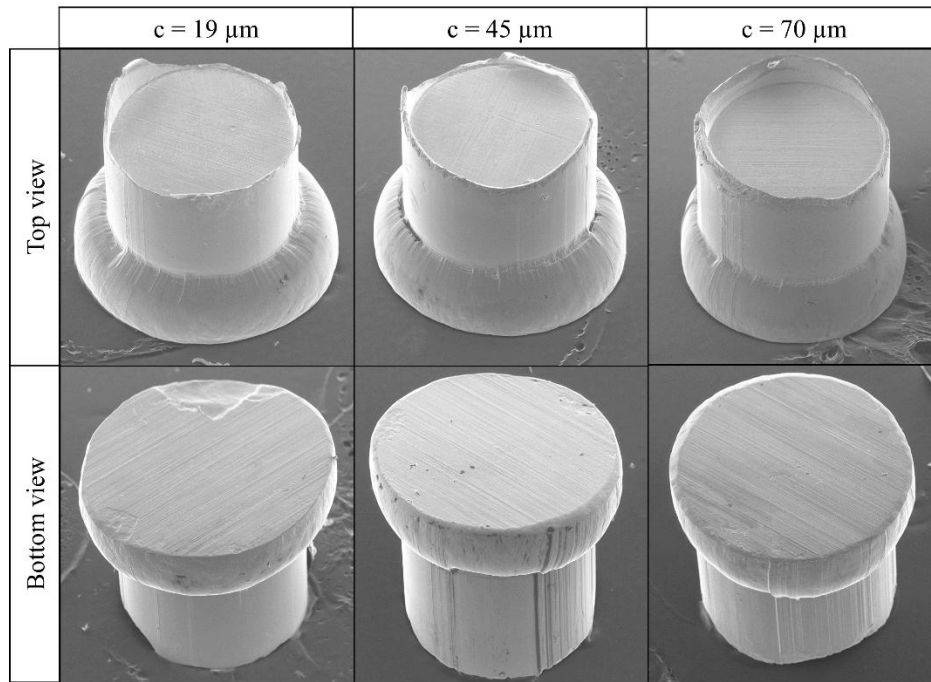
Fig. 16 Micro plug parts with fine-grained material (17 μm) fabricated by different punch-die clearance.

The blanked surfaces of the final parts with different grain size after micro-blanking operation are shown in **Fig. 17**. The fracture surface can be observed. The fracture mechanism on the blanked surface is related to the number of microvoids, which only occurs on the grain boundaries or inclusions. The initiation, growth and coalescence of microvoids induces the fracture and rough surface on the blanked region. The parabolic dimples on fracture region reflect the position and shape of microvoids. From this diagram, it can be seen that the number of dimples on fracture zone decreases with the increase of grain size, but the large-sized dimples appear on the fracture surface with coarse-grained material. This phenomenon was not observed in the prior studies [10, 11, 15].
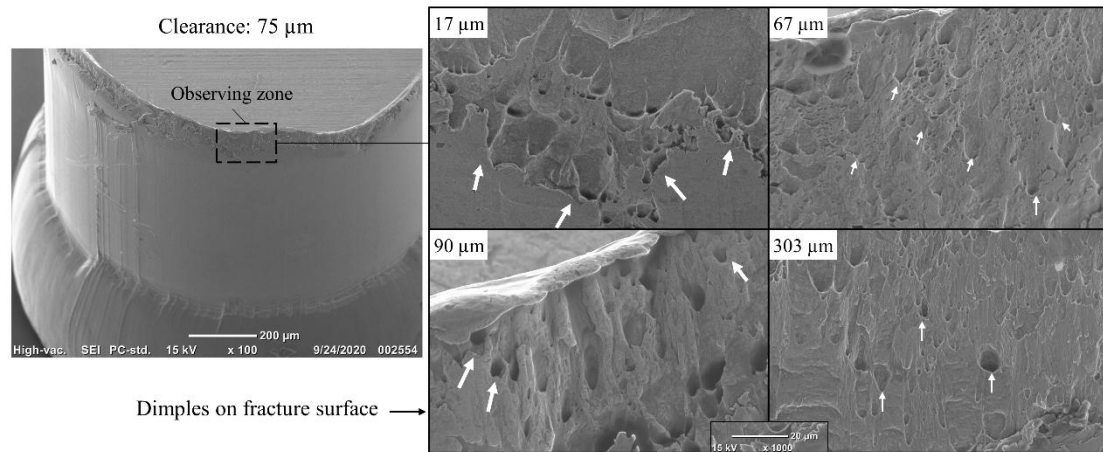
Fig. 17 Fracture surface induced by shearing deformation with different grain size.

Moreover, the morphology of the bottom surface of final parts with different grain size is shown in **Fig. 18**. The micro plug parts with grain size of 17 μm and 67 μm has a more circular geometry, but parts with the other grain sizes show more inhomogeneous. Since the larger grain size enhances individual properties of grain and the heterogeneity of whole material, inhomogeneous geometries happen on the free-form surface. The sunken area easily happens on bottom surface near the edge, which is induced by the bulge bottom after micro-blanking and uneven hardening distribution. So, at the extrusion deformation, the bottom surface could be not fully contacted to the die surface, which results in the happening of sunken area. Except the sunken area, fine-grained material shows good properties on the surface of parts. With the increase of grain size, more undesirable defects are found on the bottom surface, such as pits, crack and surface damage. The formation mechanism of pits could be related to external factors, such as dirt or impurity on specimen or die surface. Thus, during the material extrusion, the material is pushed on the die surface and extruded, the dirt or impurity on the interface of material and die surface could make damage on the part surface, then pits are formed. On the other hand, the formation of crack is based on internal factors, including strain accumulation and work hardening. When material deformation reaches a critical value, the crack may occur along grain boundaries at strain-accumulated region. It is noticed that crack is more likely to appears with coarse-grained material, since coarse-grained material has lower threshold to accumulate deformation energy. Similarly, the appearance of surface

damage is induced by an external force or item crushing the work hardening area where the region of surface reaches the ductile fracture limit due to strain accumulation. It is revealed that fine-grained material has a better surface morphology due to its better ductility than coarse-grained material.
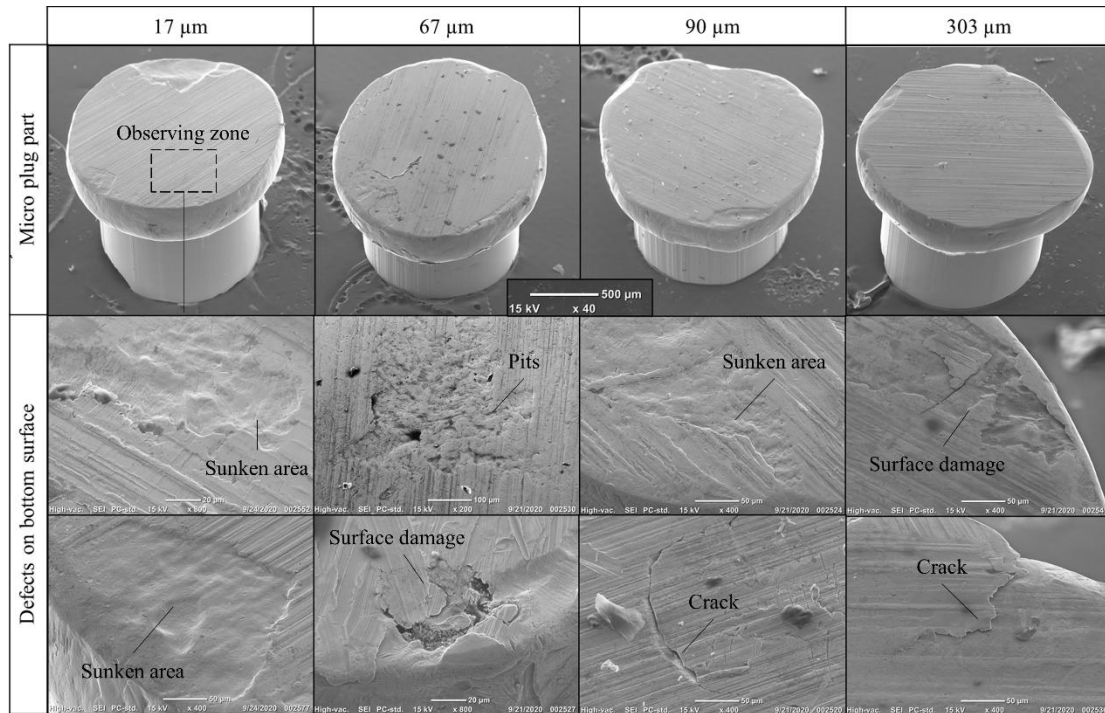
Fig. 18 Defects on bottom surface with different grain size.

In addition, **Fig. 19** focuses on the surface defects on the bulge surface with different grain size. It can be found that crack on the bulge surface is unavoidable, since the heading feature is subjected to severe deformation after shearing and extrusion deformation causing large strain accumulation and work hardening. If the crack initiates on the shearing surface after the micro-blanking operation, it will be extended in width direction after micro-heading operation due to the lateral stress. Compared to the thin and regular heading-formed crack, the heading-extended cracks are wide and warping.

To facilitate a better forming quality, a dust-free forming condition and a smoother die could be considered to reduce the externality inducing surface defects, and properly warm forming could improve the strain and damage accumulation.
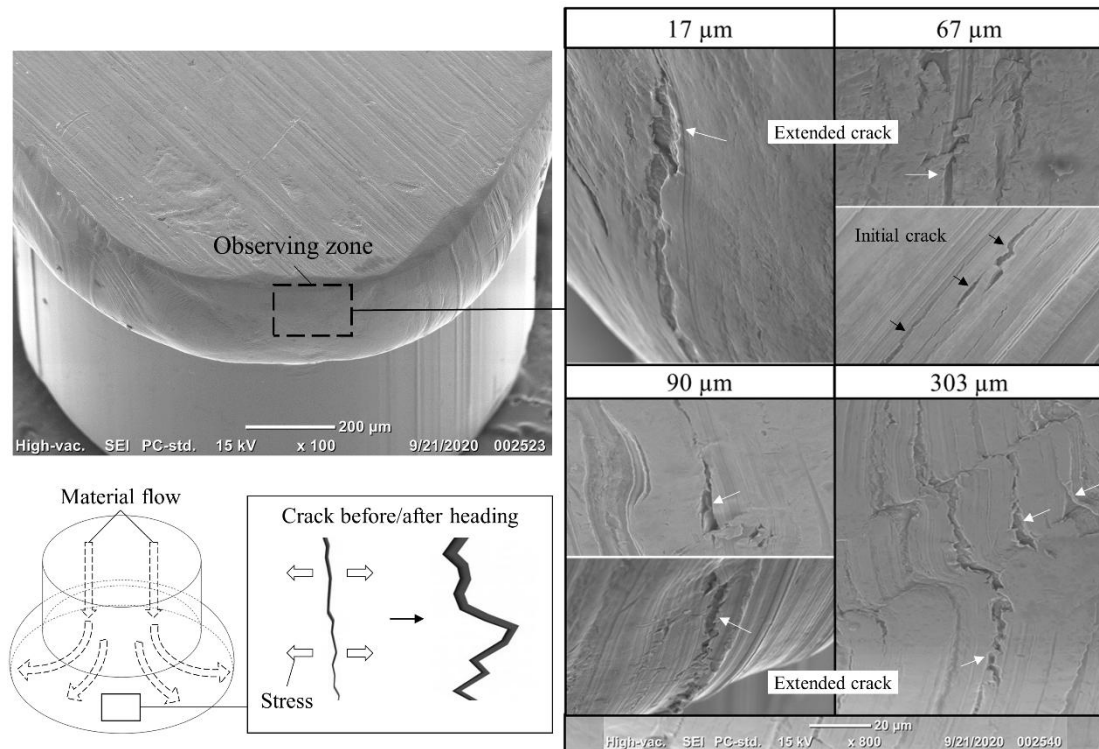
Fig. 19 Crack formation on the bulge surface with different grain size.

4. Conclusion

In this study, a novel compound microforming system is designed and established for the fabrication of micro-plug parts by directly using sheet metal. The experimental and numerical investigations are conducted from several aspects including forming load in process and microstructural evolution, geometrical precision, surface defects and radius variation of final parts considering grain size effect and the geometrical size effect of punch-die clearance. The following conclusions can be drawn from this study:

1) The novel compound microforming system combines micro-blanking and micro-heading operation, which makes it possible to fabricate plug-shaped parts from sheet metals within one single punch stroke. Sheet-based bulk microforming also facilitates the positioning, transforming and ejection operations to promote efficiency, which has potential for mass production.

2) The load-stroke curves are divided into blanking, transition and two heading

stages. The finer grains and thicker punch-die clearance can increase the forming load. When the ratio of clearance to grain size (c/d) equals one, the maximum ultimate shear stress in the blanking stage is obtained.

3) Three shear bands and three dead metal zones are recognized on the cross-section of final parts based on hardness tests, microstructure observation and simulated strain distribution. With the variation of grain size and punch-die clearance, the area of different characteristic zones changes. Based on the results, it is indicated that the material in mid-center flows to the shearing area during blanking operation, then the material in bottom center is extruded along lateral direction to die edge during heading operation.

4) The width of burr is directly related to the punch-die clearance, and it is barely affected by grain size effect. The height of burr generally reaches the maximum value when c/d equals one. The volume of burr usually increases with larger punch-die clearance, which further induces a higher shortage fraction with the interactive effect of increasing grain size.

5) The height and cylindrical diameter of the final parts change little with grain size or punch-die clearance, but bulge diameter is diminished with larger grain size and clearance. The variation of bulge diameter in peripheral direction is predicted well with CPFEM simulation.

6) Surface defects on the final parts, including fracture surface with dimples near the top edge, sunken area, pits, crack and surface damage on the bottom surface, and crack on the bulge surface are observed, and their formation mechanisms are analyzed. An improved die with smoother surface, cleaner processing condition and warm forming can be considered to eliminate the undesirable surface defects. In addition, coarse-grained material enhances the inhomogeneity for freeform shape.

In summary, a relative finer grains and a smaller punch-die clearance can promote the quality of the final parts and avoid material shortage, but the ratio of

punch-die clearance to grain size should be select properly to avoid higher ultimate shearing stress and worse burr formation.

5.   Acknowledgement

6.   Reference

[1] Y. Qin, Overview of micro-manufacturing, in: Micromanufacturing Engineering and Technology, 2015, pp. 1-34.

[2] B. Boswell, M.N. Islam, I.J. Davies, A review of micro-mechanical cutting, The International Journal of Advanced Manufacturing Technology, 94 (2017) 789-806.

[3] T. Masuzawa, State of the art of micromachining, Cirp Annals, 49 (2000) 473-488.

[4] E. Uhlmann, M. Röhner, M. Langmack, T.-M. Schimmelpfennig, Chapter 4 - Micro-electrical Discharge Machining, in: Y. Qin (Ed.) Micromanufacturing Engineering and Technology (Second Edition), William Andrew Publishing, Boston, 2015, pp. 81-105.

[5] A. Pimpin, W. Srituravanich, Review on micro-and nanolithography techniques and their applications, Engineering Journal, 16 (2012) 37-56.

[6] J. Cao, E. Brinksmeier, M. Fu, R.X. Gao, B. Liang, M. Merklein, M. Schmidt, J. Yanagimoto, Manufacturing of advanced smart tooling for metal forming, CIRP Annals, 68 (2019) 605-628.

[7] M.W. Fu, J.L. Wang, A.M. Korsunsky, A review of geometrical and microstructural size effects in micro-scale deformation processing of metallic alloy components, International Journal of Machine Tools and Manufacture, 109 (2016) 94-125.

[8] J. Xu, X. Wang, C. Wang, L. Yuan, W. Chen, J. Bao, Q. Su, Z. Xu, C. Wang, Z. Wang, D. Shan, B. Guo, A Review on Micro/Nanoforming to Fabricate 3D Metallic Structures, Advanced Materials, n/a (2020) 2000893.

[9] J.Y. Zheng, H.P. Yang, M.W. Fu, C. Ng, Study on size effect affected progressive microforming of conical flanged parts directly using sheet metals, J Mater Process Tech, 272 (2019) 72-86.

[10] M.W. Fu, W.L. Chan, Micro-scaled progressive forming of bulk micropart

via directly using sheet metals, Mater Design, 49 (2013) 774-783.

[11] B. Meng, M.W. Fu, C.M. Fu, K.S. Chen, Ductile fracture and deformation behavior in progressive microforming, Mater Design, 83 (2015) 14-25.

[12] B. Meng, M.W. Fu, S.Q. Shi, Deformation characteristic and geometrical size effect in continuous manufacturing of cylindrical and variable-thickness flanged microparts, J Mater Process Tech, 252 (2018) 546-558.

[13] X.F. Tang, S.Q. Shi, M.W. Fu, Interactive effect of grain size and crystal structure on deformation behavior in progressive micro-scaled deformation of metallic materials, Int J Mach Tool Manu, 148 (2020).

[14] J.-Y. Zheng, S.Q. Shi, M.W. Fu, Progressive microforming of pin-shaped plunger parts and the grain size effect on its forming quality, Mater Design, 187 (2020) 108386.

[15] J.-Y. Zheng, M.-W. Fu, Progressive and Compound Forming for Producing Plunger-Typed Microparts by Using Sheet Metal, Journal of Micro and Nano-Manufacturing, 8 (2020).

[16] J. Ran, L. Xu, J. Wang, T. Xu, F. Gong, Influence of dead metal zone on dislocation strengthening effect during micro-progressive forming, The International Journal of Advanced Manufacturing Technology, (2019) 1-13.

[17] M.W. Fu, B. Yang, W.L. Chan, Experimental and simulation studies of micro blanking and deep drawing compound process using copper sheet, J Mater Process Tech, 213 (2013) 101-110.

[18] W.L. Chan, M.W. Fu, J. Lu, Experimental and simulation study of deformation behavior in micro-compound extrusion process, Mater Design, 32 (2011) 525-534.

[19] F. Vollertsen, D. Biermann, H.N. Hansen, I.S. Jawahir, K. Kuzman, Size effects in manufacturing of metallic components, Cirp Ann-Manuf Techn, 58 (2009) 566-587.

[20] W.L. Chan, M.W. Fu, Experimental studies of plastic deformation behaviors in microheading process, J Mater Process Tech, 212 (2012) 1501-1512.

[21] X. Chen, Z. Wang, J. Xu, Y. Wang, J. Li, H. Liu, Sustainable production of micro gears combining micro reciprocated wire electrical discharge machining and precision forging, Journal of Cleaner Production, 188 (2018) 1-11.

[22] Q. Su, J. Xu, H. Yu, L. Shi, D. Shan, B. Guo, Effect of Grain Size on Formability and Deformation Mechanism of High-Purity Aluminum during Micro-Embossing Process at Elevated Temperature, Advanced Engineering Materials, 21 (2019) 1900690.

[23] H. Sato, K. Manabe, K. Ito, D. Wei, Z. Jiang, Development of servo-type micro-hydromechanical deep-drawing apparatus and micro deep-drawing experiments

of circular cups, J Mater Process Tech, 224 (2015) 233-239.

[24] C.J. Wang, L.D. Cheng, Y. Liu, H. Zhang, Y. Wang, D.B. Shan, B. Guo, Research on micro-deep drawing process of concial part with ultra-thin copper foil using multi-layered DLC film-coated die, The International Journal of Advanced Manufacturing Technology, 100 (2019) 569-575.

[25] N. Guo, J. Wang, C.Y. Sun, Y.F. Zhang, M.W. Fu, Analysis of size dependent earing evolution in micro deep drawing of TWIP steel by using crystal plasticity modeling, Int J Mech Sci, 165 (2020) 105200.

[26] Y. Lou, X. Liu, J. He, M. Long, Ultrasonic-assisted extrusion of ZK60Mg alloy micropins at room temperature, Ultrasonics, 83 (2018) 194-202.

[27] F. Roters, P. Eisenlohr, L. Hantcherli, D.D. Tjahjanto, T.R. Bieler, D. Raabe, Overview of constitutive laws, kinematics, homogenization and multiscale methods in crystal plasticity finite-element modeling: Theory, experiments, applications, Acta Mater, 58 (2010) 1152-1211.

[28] T. Yalçinkaya, A. Demirci, I. Simonovski, İ. Özdemir, Micromechanical Modelling of Size Effects in Microforming, Procedia Engineering, 207 (2017) 998-1003.

[29] H. Zhang, M. Diehl, F. Roters, D. Raabe, A virtual laboratory using high resolution crystal plasticity simulations to determine the initial yield surface for sheet metal forming operations, Int J Plasticity, 80 (2016) 111-138.

[30] S. Ghosh, J. Cheng, Adaptive multi-time-domain subcycling for crystal plasticity FE modeling of discrete twin evolution, Computational Mechanics, 61 (2018) 33-54.

[31] Z.Y. Cai, B. Meng, M. Wan, X.D. Wu, M.W. Fu, A modified yield function for modeling of the evolving yielding behavior and micro-mechanism in biaxial deformation of sheet metals, Int J Plasticity, 129 (2020) 102707.

[32] Z. Wang, J. Zhang, Z. Xu, J. Zhang, H.u. Hassan, G. Li, H. Zhang, A. Hartmaier, F. Fang, Y. Yan, T. Sun, Crystal plasticity finite element modeling and simulation of diamond cutting of polycrystalline copper, Journal of Manufacturing Processes, 38 (2019) 187-195.

[33] T. Fischer, E. Werner, S. Ulan kyzy, O. Munz, Crystal plasticity modeling of polycrystalline Ni-base superalloy honeycombs under combined thermo-mechanical loading, Continuum Mechanics and Thermodynamics, 31 (2019) 703-713.

[34] R. Armstrong, I. Codd, R.M. Douthwaite, N.J. Petch, The plastic deformation of polycrystalline aggregates, The Philosophical Magazine: A Journal of Theoretical Experimental and Applied Physics, 7 (1962) 45-58.

[35] R.J. Asaro, Micromechanics of crystals and polycrystals, Advances in applied mechanics, 23 (1983) 115.

[36] J. Pan, J.R. Rice, Rate sensitivity of plastic flow and implications for yield-surface vertices, International Journal of Solids and Structures, 19 (1983) 973-987.

[37] S.R. Kalidindi, C.A. Bronkhorst, L. Anand, Crystallographic texture evolution in bulk deformation processing of FCC metals, J Mech Phys Solids, 40 (1992) 537-569.

[38] M. Kardan-Halvaei, M. Morovvati, B. Mollaei-Dariani, Crystal plasticity finite element simulation and experimental investigation of the micro-upsetting process of OFHC copper, Journal of Micromechanics and Microengineering, 30 (2020) 075005.

[39] M.W. Fu, W.L. Chan, Micro-scaled products development via microforming, 2014.

[40] J. Xu, J. Li, L. Shi, D. Shan, B. Guo, Effects of temperature, strain rate and specimen size on the deformation behaviors at micro/meso-scale in ultrafine-grained pure Al, Mater Charact, 109 (2015) 181-188.

[41] E. Taupin, J. Breitling, W.-t. Wu, T. Altan, Material fracture and burr formation in blanking results of FEM simulations and comparison with experiments, J Mater Process Tech, 59 (1996) 68-78.

[42] S.K. Maiti, A.A. Ambekar, U.P. Singh, P.P. Date, K. Narasimhan, Assessment of influence of some process parameters on sheet metal blanking, J Mater Process Tech, 102 (2000) 249-256.

[43] W. Zhou, J. Lin, T.A. Dean, L. Wang, Analysis and modelling of a novel process for extruding curved metal alloy profiles, Int J Mech Sci, 138-139 (2018) 524-536.

[44] E. Ghassemali, A.E.W. Jarfors, M.J. Tan, S.C.V. Lim, On the microstructure of micro-pins manufactured by a novel progressive microforming process, Int J Mater Form, 6 (2013) 65-74.

[45] S.Z. Qamar, Shape Complexity, Metal Flow, and Dead Metal Zone in Cold Extrusion, Materials and Manufacturing Processes, 25 (2010) 1454-1461.

[46] B. Meng, M.W. Fu, C.M. Fu, J.L. Wang, Multivariable analysis of micro shearing process customized for progressive forming of micro-parts, Int J Mech Sci, 93 (2015) 191-203.